Experimental and theoretical investigations of laser-induced crystallization and amorphization in phase-change optical recording media

Cite as: Journal of Applied Physics **82**, 4183 (1997); https://doi.org/10.1063/1.366220
Submitted: 13 June 1997 . Accepted: 04 August 1997 . Published Online: 17 August 1998

Chubing Peng, Lu Cheng, and M. Mansuripur

Experimental and theoretical investigations of laser-induced crystallization and amorphization in phase-change optical recording media

Chubing Peng,[a] Lu Cheng, and M. Mansuripur
Optical Sciences Center, The University of Arizona, Tucson, Arizona 85721

(Received 13 June 1997; accepted for publication 4 August 1997)

We describe the numerical procedure for calculating three-dimensional profiles of temperature in a multilayer stack illuminated by a laser beam, and model the crystallization and amorphization kinetics for phase-change rewritable media. Experimental methods have been used to determine indirectly the probabilities of nucleation and growth for $Ge_2Sb_2Te_5$ alloy. Some of the fundamental behaviors of phase-change erasable media, such as the crystallization of as-deposited amorphous phase, amorphization of supercooled liquid, and recrystallization of quenched amorphous phase, have been illustrated based on our three-dimensional temperature calculations and the model kinetics. The calculated transient reflectance behavior of as-deposited $Ge_2Sb_2Te_5$ amorphous films in a single layer and in a quadrilayer stack, as well as the erasure behavior of $Ge_2Sb_2Te_5$ alloy in a quadrilayer disk are in good agreement with experimental observations. © *1997 American Institute of Physics.* [S0021-8979(97)07821-3]

I. INTRODUCTION

In rewritable phase-change optical recording, a bit of information is written by applying a short pulse of a focused laser beam to a crystallized area of the disk. This pulse increases the local temperature of the storage layer above its melting point. When the pulse ends, the molten spot cools at rates approaching 10^9-10^{10} °C/s, and subsequently amorphizes. The mark can later be identified by using the same focused laser beam at a much lower incident power to measure the reflection (or transmission) of the spot relative to its crystalline surroundings. Erasure is achieved by exposing the film to intermediate levels of laser power, raising the local temperature of the storage layer above its crystallization but below the melting temperature. The amorphous mark thus recrystallizes while the surrounding crystalline matrix remains largely unaffected, and the optical contrast is removed.[1–6] The amorphization and crystallization behavior of the storage layer is therefore fundamental to phase-change recording.

Extensive experimental studies have been conducted to understand the crystallization phenomenon of phase-change materials.[7–10] Computer simulations have also been proposed to calculate the time dependence of the temperature distribution,[11] and to analyze the overwrite process for phase-change media.[12,13] In these simulations,[12,13] however, the nucleation and growth processes were not distinguished and crystallization was characterized by a single timescale. The Johnson–Mehl–Avrami (JMA) equation,[6] which describes the crystallized fraction as a function of time during isothermal annealing, has been extended to nonuniform and transient thermal processes. Certain observed features, such as the recrystallization of amorphous marks through the growth of their crystalline edges towards the center,[10,14] however, cannot be discussed in these models.

In this paper we describe a theoretical model for simulating the writing and erasing processes of phase-change media by taking into account temperature distributions in three-dimensional space, crystallization of amorphous marks by nucleation and growth, phase transition from solid (crystalline or amorphous) to liquid state, and formation of amorphous marks by quenching from melt. We also show results of certain experiments that appear to confirm the predictions of our model.

II. SIMULATION METHOD

A. Laser-induced temperature distribution in a multilayer stack

Phase-change disks generally consist of an N-layer stack deposited on a substrate, where each layer has different optical and thermal properties. (Here it is convenient to regard the substrate as the zeroth layer.) Let x, y, and z be the axes in a Cartesian coordinate system, with x and y parallel to the plane of the film while the positive z axis goes through the film and into the substrate. Starting at time $t=0$ and at $(x,y)=(x_0,0)$ a sharply focused, circularly symmetric, Gaussian beam of light illuminates the media from either the surface side or the substrate side. The focused beam is assumed to move along the x axis at a linear velocity of V. The incident intensity distribution can therefore be written as

$$I(x,y,t)=[P_0(t)/(\pi r_0^2)]\exp\{-[(x-x_0-Vt)^2+y^2]/r_0^2\}. \quad (1)$$

Here r_0 is the $1/e$ radius of the Gaussian beam and $P_0(t)$ is its instantaneous optical power. Denoting $T(x,y,z,t)$ the temperature increase above the ambient, and assuming that heat loss from the surface $(z=0)$ is proportional to $T(x,y,z=0,t)$, one obtains the following heat transfer equation[15]

$$C_n\frac{\partial T}{\partial t}=K_n\Delta^2 T+g, \quad n=0,1,2,...,N \quad (2)$$

with the following boundary conditions

[a]Electronic mail: cpeng@u.arizona.edu

$$T(x=\pm\infty,y,z,t)=0, \tag{3a}$$

$$\frac{\partial T(x,y=0,z,t)}{\partial y}=0, \tag{3b}$$

$$T(x,y=\infty,z,t)=0, \tag{3c}$$

$$\frac{\partial T(x,y,z=0,t)}{\partial z}=\gamma T(x,y,z=0,t), \tag{3d}$$

$$T(x,y,z=\infty,t)=0. \tag{3e}$$

Continuity conditions at the interface ($z=z_n$) between adjacent layers (nth and $n-1$st) requires that

$$T(x,y,z=z_n^+,t)=T(x,y,z,=z_n^-,t), \tag{3f}$$

$$K_n\frac{\partial T(x,y,z_{n,}^+,t)}{\partial z}=K_{n-1}\frac{\partial T(x,y,z_n^-,t)}{\partial z}. \tag{3g}$$

In Eqs. (2) and (3), C_n is the specific heat and K_n the thermal conductivity of the nth layer, g is the absorbed optical energy per unit time per unit volume converted to heat, and γ is a constant that controls the rate of heat flow from the surface of the stack. Light absorption by the films is assumed to be the main source of thermal energy. In phase-change media, the three phases (namely, crystalline, amorphous, and liquid) encountered in the process of recording may have different absorption coefficients because they usually have different optical properties. In addition, exothermic heat from amorphous to crystalline phase transition and also from liquid to solid transformation (either crystalline or amorphous) is the other source of thermal energy.

A number of numerical procedures have been developed for solving the thermal diffusion equation.[16–19] The exact solution of the heat diffusion equation in frequency space has also been reported.[20,21] Here, because of the complexity of the problem, we believe that the alternating direction-implicit technique is an efficient way to handle Eqs. (2) and (3). But the obvious generalization of the implicit technique described in Ref. 16 to three spatial variables is not going to be stable for a large ratio of the time increment (Δt) to the square of the space increments ($\Delta x^2,\Delta y^2,\Delta z^2$) for typical multilayer structures. Nevertheless, it is still possible to obtain stable solutions by reformulating the Crank–Nicolson finite difference equation in three dimensions.[22] In this technique, the temperature increase in going from t to $t+\Delta t$ is evaluated using three steps. Table I lists the basic equations for an N-layer multilayer stack. In this table, ${}_{ix}^{iy}T_j^k$ stands for the approximation to temperature at $(x,y,z,t)=[(ix-0.5ix_{\max})\times\Delta x,iy\times\Delta x,j\times\Delta z,k\Delta t]$, (for each layer we can have a different value of Δz_n in the z direction); ${}_{ix}^{iy}T_j^{k+1}$ (1) and ${}_{ix}^{iy}T_j^{k+1}$ (2) are the intermediate solutions from t to $t+\Delta t$; $D_n=K_n/C_n$ is the diffusivity of layer n; L is the released exothermic heat when the phase-change layer is transformed from amorphous to crystalline phase or from liquid to solid; and Y is the rate of flow of energy through the multilayer, which was given in Ref. 16.

When the temperature of the phase-change layer reaches the melting point, T_m, the absorbed optical energy will keep the temperature of that layer at the melting point (superheating is neglected here), while, at the same time, it increases the enthalpy of the phase-change alloy. When the increased enthalpy becomes greater than the latent heat, the solid-to-liquid phase transition occurs. After the phase transformation, the temperature rises once again.

One should note that, in the equations of Table I, temperature variations of the thermal constants C_n and K_n are not considered, but these can easily be included. The thermal constants of very thin films, especially their thermal conductivities, have been found to be considerably different from those of the bulk materials.[23] Reliable temperature dependence for these constants are not available at the present time.

B. Crystallization model

For the kinetics of crystallization of the amorphous phase and solidification of molten regions, we use the standard theory of kinetics in our simulations.[24] In both cases, crystallization occurs either by the nucleation of critical size particles and their subsequent growth within the untransformed region, or by the growth of crystallites at the boundary between the untransformed region and the surrounding crystalline matrix. For the purpose of these simulations, the phase-change layer is discretized into an array of square tiles, each tile having dimensions $\Delta\times\Delta\times d$, where Δ is the size of tile along x and y axes, and d is the thickness of the phase-change layer. Δ is chosen to be comparable to the critical size of nuclei at the temperature at which nucleation rate is maximum. There is no physical reason for the particular tile geometry chosen here and, in fact, irregular tiles would have been preferable if computational complexity were not a concern. We do not delve into this matter further since the objective is merely to show the feasibility of the concept with the least complicated model and to explain the gross features of the phenomena observed in real films.

Neglecting the time dependence of the nucleation rate,[25] the probability for an untransformed tile (either in amorphous state or in supercooled liquid state) to become a crystalline nucleus during time interval Δt is given by

$$P_n=\alpha\Delta t\,\exp\{-\beta[E_{a1}+A/(\Delta G)^2]\}. \tag{4}$$

In Eq. (4), α is a frequency factor related to atomic vibrations; $\beta=1/k_BT$, where k_B is the Boltzmann constant, and T is the absolute temperature of the tile; E_{a1} is the activation energy associated with nucleation; ΔG is the excess Gibbs free energy of the amorphous phase (or the supercooled liquid) over the crystalline solid; A is related to interfacial surface free energy between amorphous phase (or liquid phase) and crystalline phase. $A/(\Delta G)^2$ in Eq. (4) is the excess free energy for the formation of a stable nucleus.

Alternatively, an untransformed tile may become crystalline by growing from an adjacent nucleus or from the boundary of the surrounding crystalline regions. The growth velocity (V_g) of small crystallites may be expressed as

TABLE I. Basic equations for solving the thermal diffusion equation in multilayers in three-dimensional space.

Part I. First step (z implicit, x and y explicit)

$$B_1^{(0)}\ {}^{iy}_{ix}T_0^{k+1}(1)+(B_0^{(0)}+B_2^{(0)})\ {}^{iy}_{ix}T_1^{k+1}(1)=B_3^{(ix,iy,0,k)};\quad 1\leqslant ix\leqslant ix_{\max}-1,\ 0\leqslant iy\leqslant iy_{\max}-1 \tag{T1}$$

$$B_0^{(j)}\ {}^{iy}_{ix}T_{j-1}^{k+1}(1)+B_1^{(j)}\ {}^{iy}_{ix}T_j^{k+1}(1)+B_2^{(j)}\ {}^{iy}_{ix}T_{j+1}^{k+1}(1)=B_3^{(ix,iy,j,k)}; \tag{T2}$$
$$1\leqslant ix\leqslant ix_{\max}-1,\ 0\leqslant iy\leqslant iy_{\max}-1,\ 0<j\leqslant j_{\max}-1$$

$$B_0^{(0)}=-D_N(\Delta x/\Delta z_N)^2;$$

$$B_0^{(j)}=-D_n(\Delta x/\Delta z_n)^2;\ \text{if } j \text{ belongs to layer } n \tag{T3}$$

$$B_0^{(j)}=-2D_n(\Delta x/\Delta z_n)^2/[1+(C_{n-1}/C_n)(\Delta z_{n-1}/\Delta z_n)];\ \text{if } j \text{ belongs to the interface}$$

$$B_2^{(0)}=-D_N(\Delta x/\Delta z_N)^2;$$

$$B_2^{(j)}=-D_n(\Delta x/\Delta z_n)^2;\ \text{if } j \text{ belongs to layer } n \tag{T4}$$

$$B_2^{(j)}=-2D_{n-1}(\Delta x/\Delta z_n)^2(C_{n-1}/C_n)(\Delta z_n/\Delta z_{n-1})\times[1+(C_{n-1}/C_n)(\Delta z_{n-1}/\Delta z_n)]^{-1};\ \text{if } j \text{ belongs to the interface}$$

$$B_1^{(0)}=2(\Delta x)^2/\Delta t-(B_0^{(0)}+B_2^{(0)})(1+\gamma\Delta z_N) \tag{T5}$$

$$B_1^{(j)}=2(\Delta x)^2/\Delta t-(B_0^{(j)}+B_2^{(j)});\ \text{if } j\neq 0$$

$$\begin{aligned}B_3^{(ix,iy,0,k)}=&2E_n[{}^{iy}_{ix-1}T_0^k+{}^{iy}_{ix+1}T_0^k+{}^{iy-1}_{ix}T_0^k+{}^{iy+1}_{ix}T_0^k]\\&+[4(\Delta x)^2/\Delta t-8E_n-B_1^{(j)}]\ {}^{iy}_{ix}T_0^k-[B_0^{(0)}+B_2^{(0)}]\ {}^{iy}_{ix}T_1^k\\&+4[Y(0)-Y(0.5\Delta z_n)](\Delta z_N C_N\Delta t)^{-1}G(ix,iy,k)\left[\int_{k\Delta t}^{(k+1)\Delta t}P_0(t)dt\right]+2L_j;\quad if\ \ j=0\end{aligned} \tag{T6}$$

$$\begin{aligned}B_3^{(ix,iy,j,k)}=&2E_n[{}^{iy}_{ix-1}T_j^k+{}^{iy}_{ix+1}T_j^k+{}^{iy-1}_{ix}T_j^k+{}^{iy+1}_{ix}T_j^k]\\&+[4(\Delta x)^2/\Delta t-8E_n-B_1^{(j)}]\ {}^{iy}_{ix}T_j^k-B_0^{(j)}\ {}^{iy}_{ix}T_{j-1}^k-B_2^{(j)}\ {}^{iy}_{ix}T_{j+1}^k\\&+2\{Y[(j-0.5)\Delta z_n]-Y[(j+0.5)\Delta z_n]\}(\Delta z_n C_n\Delta t)^{-1}G(ix,iy,k)\\&\times\left[\int_{k\Delta t}^{(k+1)\Delta t}P_0(t)dt\right]+2L_j;\quad \text{if } j\neq 0 \text{ and } j \text{ belongs to layer n}\end{aligned}$$

$$\begin{aligned}B_3^{(ix,iy,j,k)}=&2E_n[{}^{iy}_{ix-1}T_j^k+{}^{iy}_{ix+1}T_j^k+{}^{iy-1}_{ix}T_j^k+{}^{iy+1}_{ix}T_j^k]\\&+[4(\Delta x)^2/\Delta t-8E_n-B_1^{(j)}]\ {}^{iy}_{ix}T_j^k-B_0^{(j)}\ {}^{iy}_{ix}T_{j-1}^k-B_2^{(j)}\ {}^{iy}_{ix}T_{j+1}^k\\&+2\{Y[(j-0.5)\Delta z_n]-Y[(j+0.5)\Delta z_n]\}[0.5(C_n\Delta z_n+C_{n-1}\Delta z_{n-1})\Delta t]^{-1}\\&\times G(ix,iy,k)\left[\int_{k\Delta t}^{(k+1)\Delta t}P_0(t)dt\right]+2L_j;\quad if\ \ j\neq 0 \text{ and } j \text{ belongs to the interface}\end{aligned}$$

where E_n, $G(ix,iy,k)$, and L are defined as

$$E_n=D_n;\ \text{if } j \text{ belongs to the layer } n; \tag{T7}$$

$E_n=[D_n+(\Delta z_{n-1}/\Delta z_n)(C_{n-1}/C_n)D_{n-1}][1+(\Delta z_{n-1}/\Delta z_n)(C_{n-1}/C_n)]^{-1}$; if j belongs to the interface, and $j\neq 0$;

$$E_n=D_N;\ \text{if } j=0;$$

$$G(ix,iy,k)=\int_{(ix-0.5)\Delta x}^{(ix+0.5)\Delta x}dx\int_{(iy-0.5)\Delta x}^{(iy+0.5)\Delta x}dy(\pi r_0^2)^{-1}\ \exp(\{[x-x_0-(k-0.5)V\Delta t]^2+y^2\}/r_0^2) \tag{T8}$$

$L_j=L(\Delta x)^2\Delta z_n(C_n\Delta z_n+C_{n+1}\Delta z_{n+1})^{-1}$; if j belongs to the interface between the phase-change layer n and the upper layer $n+1$, $j\neq 0$; (T9)

$L_j=L(\Delta x)^2(C_n)^{-1}$; if j belongs to the phase-change layer n; or, if j belongs to the interface between the phase-change layer n and air ($j=0$);

$L_j=L(\Delta x)^2\Delta z_n(C_n\Delta z_n+C_{n-1}\Delta z_{n-1})^{-1}$; if j belongs to the interface between the phase-change layer n and the lower layer $(n-1)$;

$L_j=0$; otherwise.

Part II. Second step (y implicit, z and x explicit)

$$B_1^{(j)}\ {}^{0}_{ix}T_j^{k+1}(2)+[B_0^{(j)}+B_2^{(j)}]\ {}^{1}_{ix}T_j^{k+1}(2)=B_3^{(ix,0,j,k)};\quad 1\leqslant ix\leqslant ix_{\max}-1,\ 0\leqslant j\leqslant j_{\max}-1 \tag{T9}$$

$$B_0^{(j)}\ {}^{iy-1}_{ix}T_j^{k+1}(2)+B_1^{(j)}\ {}^{iy}_{ix}T_j^{k+1}(2)+B_2^{(j)}\ {}^{iy+1}_{ix}T_j^{k+1}(2)=B_3^{(ix,iy,j,k)}; \tag{T10}$$
$$1\leqslant ix\leqslant ix_{\max}-1,\ 1\leqslant iy\leqslant iy_{\max}-1,\ 0\leqslant j\leqslant j_{\max}-1$$

$$B_0^{(j)}=B_2^{(j)}=-E_n; \tag{T11}$$

$$B_1^{(j)}=2[E_n+(\Delta x)^2/\Delta t]; \tag{T12}$$

$$B_3^{(ix,0,j,k)}=-2E_n({}^{1}_{ix}T_j^k-{}^{0}_{ix}T_j^k)+2(\Delta x)^2(\Delta t)^{-1}\ {}^{0}_{ix}T_j^{k+1}(1) \tag{T13}$$

$$B_3^{(ix,iy,j,k)}=-E_n({}^{iy-1}_{ix}T_j^k-2\ {}^{iy}_{ix}T_j^k+{}^{iy+1}_{ix}T_j^k)+2(\Delta x)^2(\Delta t)^{-1}\ {}^{iy}_{ix}T_j^{k+1}(1)$$

E_n is given in Part I.

Part III. Third step (x implicit, y and z explicit)

$$B_0^{(j)}\ {}^{iy}_{ix-1}T_j^{k+1}+B_1^{(j)}\ {}^{iy}_{ix}T_j^{k+1}+B_2^{(j)}\ {}^{iy}_{ix+1}T_j^{k+1}(2)=B_3^{(ix,iy,j,k)}; \tag{T14}$$
$$1\leqslant ix\leqslant ix_{\max}-1,\ 0\leqslant iy\leqslant iy_{\max}-1,\ 0\leqslant j\leqslant j_{\max}-1$$

$$B_0^{(j)}=B_2^{(j)}=-E_n; \tag{T15}$$

$$B_1^{(j)}=2[E_n+(\Delta x)^2/\Delta t]; \tag{T16}$$

$$B_3^{(ix,ty,j,k)}=-E_n({}^{iy}_{ix-1}T_j^k-2\ {}^{iy}_{ix}T_j^k+{}^{iy}_{ix+1}T_j^k)+2(\Delta x)^2(\Delta t)^{-1}\ {}^{iy}_{ix}T_j^{k+1}(2) \tag{T17}$$

E_n is given in Part I.

$$V_g = f a_0 \alpha [1 - \exp(-\beta \Delta G)] \exp(-\beta E_{a2}). \quad (5)$$

Here f is a factor related to the growth mode;[26] a_0 is the atomic jump distance; and E_{a2} is the activation energy associated with diffusion of atoms. The probability of growth (P_g) for each tile during time interval Δt is hence proportional to $V_g \Delta t/\Delta$.

In Eqs. (4) and (5), A, ΔG, and f are usually temperature dependent. For simplicity, we assume that A is tempera ture independent, in which case its value may be determined from the peak temperature (T_N) at which the nucleation rate is a maximum. The temperature dependence of ΔG may be approximated by[27]

$$\Delta G = \begin{cases} \Delta H_2 \left[1 - \dfrac{T}{T_g} \left(1 - \dfrac{\Delta H_1}{\Delta H_2} \dfrac{T_m - T_g}{T_m} \right) \right] & T \leqslant T_g \\ \Delta H_1 \dfrac{T_m - T}{T_m} & T > T_g \end{cases}. \quad (6)$$

Here T_m is the melting point, T_g is the glass transition temperature, ΔH_1 is the latent heat of solid-to-liquid transition; ΔH_2 is the exothermic heat of amorphous-to-crystalline transformation.

From our simulations, experimental results can be well explained if f is assumed to be proportional to $\exp[-0.8/(1-T/T_m)]$, suggesting a lateral growth mechanism[28] in the very thin phase-change layer. From these assumptions and Eq. (5), the growth probability of tile during a time interval Δt can be written as follows:

$$P_g = pa\Delta t \exp[-0.8/(1-T/T_m)] \times [1 - \exp(-\beta \Delta G)] \exp(-\beta E_{a2}), \quad (7)$$

where p may be dependent on the tile size. In Eqs. (4), (6), and (7), E_{a1}, E_{a2}, T_m, ΔH_1, and ΔH_2 may be determined from isothermal and differential scanning calorimetry (DSC) experiments,[3,8,9,11] α and p are fitted by matching the simulation results with experiments; and T_g may be assumed to be two-thirds of the melting point.[27]

In the simulations, in going from time t to $t+\Delta t$, three-dimensional temperature distribution at $t+\Delta t$ in the film is first calculated. The average temperature (T) of each tile in the array is therefore determined. Then, the array of tiles is scanned in a checkerboard fashion. Each tile has four nearest neighbors. If none of the neighbors is crystallized, the untransformed tile has a probability of nucleation P_n; otherwise, it has a probability of growth P_g. Exothermic heat released due to growth is taken into account in the temperature calculation for the next step (from $t+\Delta t$ to $t+2\Delta t$).

III. EXPERIMENTS

To probe the fundamental behavior of amorphization and crystallization involved in the processes of writing and erasure for phase-change optical storage media, a static tester and a dynamic tester were used for experiments.[29,30] In the static tester, a pulsed laser beam is brought to focus on the phase-change film by an objective lens. The amorphous film is heated and the transient reflectivity variations with time are simultaneously monitored during the heating cycle. Two samples were used for these experiments: sample 1 was a single $Ge_2Sb_2Te_5$ (GST) layer film and sample 2 consisted of a quadrilayer stack. The layer structures for these samples are tabulated in Table II.

TABLE II. Layer structures for sample 1, sample 2, and the disk used in the experiment. (PMMA means polymethyl methacrylate and PC stands for polycarbonate).

	Sample 1	Sample 2	Disk
Substrate	Flat PMMA	Flat PMMA	Grooved PC
$ZnS-SiO_2$	···	194 nm	128 nm
$Ge_2Sb_2Te_5$	85 nm	26 nm	20 nm
$ZnS-SiO_2$	···	28 nm	35 nm
Al alloy	···	120 nm	150 nm

Using the dynamic tester, writing and erasing characteristics of a phase-change disk were evaluated. The disk structure is also given in Table II. The 690 nm laser beam is focused on the disk through the polycarbonate substrate by an objective lens of NA=0.6. (NA: numerical aperture of the lens). Prior to conducting write/erase tests, the disk was initialized so that the GST alloy was in crystalline phase. In the write/erase experiments, the disk was spinning at a linear velocity of 8.8 m/s. For the measurement of erasability, the following experimental procedures were used: (1) a track was written with a 4 MHz tone of 40% duty cycle, and the rf readout signal (S_0) of the written marks was obtained; (2) the recorded track was partially erased using a cw laser at a fixed power and the readout signal (S_1) after erasure was obtained; (3) the track was fully erased at an appropriate cw laser power. The relative signal strength, S_1/S_0, as a function of erasing power was thus obtained by repeating the procedures (1)–(3). Prior to erasure, the readout signal from the written track was measured using a spectrum analyzer and was found to have a carrier-to-noise ratio (CNR) of 52 dB.

IV. RESULTS AND DISCUSSIONS

A. Probability curves and material parameters

Table III lists the kinetics parameters for the GST alloy, and Fig. 1 shows the probabilities of nucleation and growth per nanosecond for sample 1, calculated from Eqs. (4), (6),

TABLE III. Numerical values of the kinetics parameters of $Ge_2Sb_2Te_5$ alloy used in computer simulation.

Symbol	Value	Unit
E_{a1}	2.19	eV
E_{a2}	2.23	eV
T_m	616	°C
T_N	405	°C
T_g	400	°C
ΔH_1	418.9	J/cm^3
ΔH_2	218.5	J/cm^3
α	4×10^{25}	s^{-1}
p	0.87 (for sample 1) 3.69 (for sample 2) 3.69 (for the disk)	

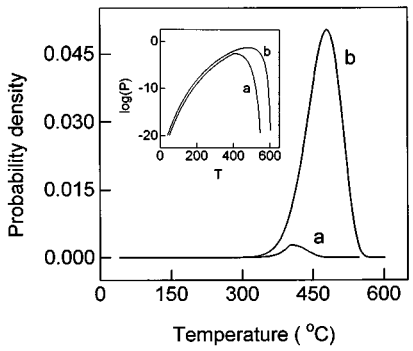

FIG. 1. Temperature (T) dependence of the probabilities (P) of nucleation and growth per nanosecond for sample 1: (a) nucleation; (b) growth. The same curves were used for sample 2 and disk, but the growth probability was scaled by a factor of 4.2. The inset is the logarithmic plots of probabilities.

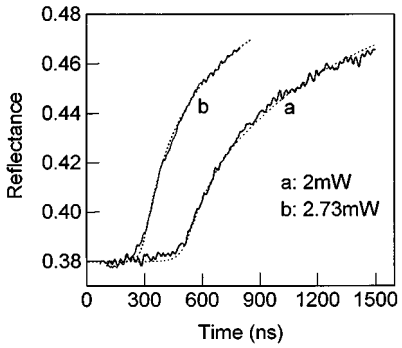

FIG. 2. Variations of reflectance with time during crystallization of an amorphous region of the sample 1 by a focused laser beam. The solid curves are obtained experimentally, and the dotted curves are simulation results. In the two experiments conducted, the laser power on the film surface was 2 mW [curve (a)] and 2.7 mW [curve (b)]. The objective lens for focus had NA=0.4 and the wavelength of the light was $\lambda = 780$ nm. For simulations, $1/e$ radius $r_0 = 960$ nm; tile size $\Delta = 4$ nm; and time interval $\Delta t = 2.5$ ns. To obtain best agreement with experimental results, we have used 95% of experimental power in the simulations.

and (7). One can see that the assumed probability of growth is larger than that of nucleation in the temperature range of interest; this means that, once small crystallites nucleate in an amorphous region (or supercooled liquid), they grow rapidly. Moreover, it is evident that both nucleation and growth rates have a maximum probability but the peak temperature for the growth rate is higher than that for the nucleation rate. From the probability curves, the crystallization temperature was estimated to be about 140 °C if the film was heated uniformly on a thermal stage at a heating rate of 10 deg/min from ambient temperature. This result is consistent with DSC experimental data.[3]

Table IV lists the thermal and optical parameters of materials used in our simulations. Among the thermal parameters, specific heat (C) is from Ref. 11; thermal conductivities of the GST alloy (in the amorphous phase), $ZnS–SiO_2$, and the Al alloy are from Ref. 29; thermal conductivity of GST (in crystalline phase) is measured in this work; and the thermal parameters of the GST alloy in liquid phase are assumed to be the same as those in crystalline phase. In Table IV, except for the refractive index of the GST alloy in liquid phase, all the optical parameters are measured. The GST alloy in liquid phase is assumed to have the same refractive index as that in the amorphous phase.[7]

B. Crystallization of as-deposited amorphous single layer film

Figure 2 shows the change of reflectance versus time during the heating process in the case where the focused beam is incident from the air side on sample 1. It is observed that the reflected light does not change initially after the film has been exposed to the light. After this initial phase, the reflectance increases with time. The onset time, at which the reflectivity of the film begins to show a noticeable change, decreases with the increase of the laser power. Figure 2 also shows the simulation results (dotted curves). It is seen that the simulation reproduces the experimental results quite well.

Figure 3 shows the evolution of temperature within the phase-change layer for the assumed laser power of 1.9 mW on sample 1. The curves labeled (a), (b), and (c) correspond to points at the center of the focused spot, 300 nm away from the center, and 600 nm away from the center, respectively. For curve (a), the temperature rises abruptly at $t = 460$ ns; the same thing happens to curve (b) around $t = 500$ ns. This is a result of exothermic heat released during the rapid growth in the interval between 460 and 600 ns [see curve (a) in Fig. 2]. (At the onset time of crystallization, the temperature is about 400 °C.) After about 100 ns, the temperature increases smoothly because absorption within the crystalline region is less than that of amorphous regions. For curve (c) in Fig. 3, the rapid increase of temperature is barely perceptible.

Figure 4 shows different stages of crystallization of sample 1 obtained by computer simulation. The assumed laser power on the film is 1.9 mW in this case. At $t = 400$ ns, one can see a few random nuclei at the center of the hot spot.

TABLE IV. Numerical values for specific heat (C), thermal conductivity (K), and complex refractive index ($\tilde{n}$) of substrate, $ZnS–SnO_2$, $Ge_2Sb_2Tb_5$, and Al alloy.

	C (J/cm^3/K)	K (J/cm/K/s)	$\tilde{n}$ (Sample 1)	$\tilde{n}$ (Sample 2)	$\tilde{n}$ (Disk)
Substrate	1.7	0.0022	1.46	1.49	1.49
GST (amorphous)	1.285	0.0017	$4.7+1.4i$	$4.39+1.53i$	$4.39+1.53i$
GST (crystalline)	1.285	0.005	$5.13+3.5i$	$4.84+3.53i$	$4.84+3.53i$
GST (liquid)	1.285	0.005	⋯	⋯	$4.39+1.53i$
$ZnS–SiO_2$	2.005	0.006	⋯	2.0	2.08
Al alloy	2.45	0.25	⋯	$1.8+6.1i$	$1.8+6.1i$

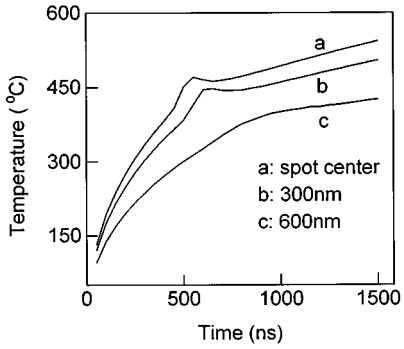

FIG. 3. Calculated temperature vs time at three different locations in the middle of the GST layer for the sample 1: (a) center of the focused spot; (b) 300 nm away from the center; (c) 600 nm away from the center. The assumed laser power is 1.9 mW in all cases.

At $t=600$ ns, the central region has been transformed to a fairly large crystalline phase. Around the boundary of this crystalline region, however, there are still many nuclei. The onset time of crystallization, about 460 ns in this case, depends on the probability of nucleation. As time evolves, the crystalline region expands. At $t=1500$ ns, the size of the crystalline region is almost equal to the $1/e$ diameter of the focused spot.

C. Crystallization of as-deposited amorphous quadrilayer film

Figure 5 displays variations of reflectance versus time for the crystallization of the amorphous film in sample 2. Before the laser pulse was turned on, a 0.78 mW continuous wave (cw) laser power was on the film for acquiring focus. Calculation shows that this cw power will produce a maximum temperature of about 55 °C at the center of the spot. This temperature is too low to result in any change such as relaxation or crystallization of the phase-change alloy. Comparing Figs. 5 and 2, it is seen that the crystallization behavior of the thin GST layer in the quadrilayer film is similar to that of the thick GST layer in the single layer film. Once

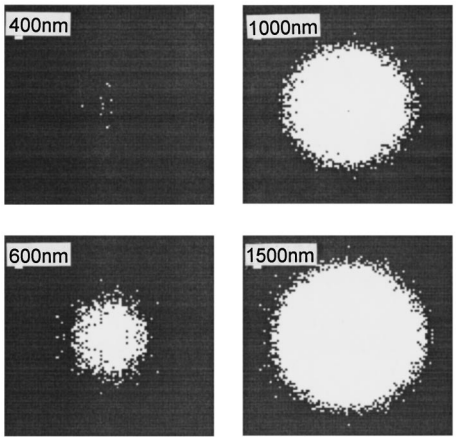

FIG. 4. Crystallization of amorphous phase caused by the irradiation of a focused, 1.9 mW laser beam. The dark region represents the amorphous phase, while the bright regions are crystalline phase. The real nuclei size (in area) are only about 1/25 of those displayed. Each frame is 2 μm$\times$2 μm.

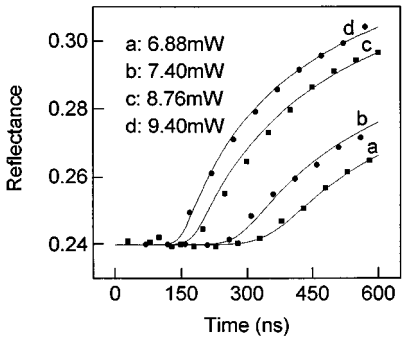

FIG. 5. Variation of reflectance with time during crystallization of an amorphous region of sample 2 by a focused laser beam. The dot and square are experimental results, and the solid curves are simulation results. Different curves correspond to different pulse power levels: (a) 6.88 mW; (b) 7.40 mW; (c) 8.76 mW; and (d) 9.40 mW. In the experiments, the objective lens used for focus had NA=0.4 and the laser wavelength was 690 nm. For simulations, $r_0=870$ nm, $p=3.69$, $\Delta=4$ nm, and $\Delta t=2.5$ ns. The magnitude of p may be approximately obtained by scaling from the 85 nm thick GST alloy of the sample 1 to the 26 nm thick GST alloy of the sample 2.

again it is seen that the calculated reflectivity reproduces the experimental data quite well within the laser power range examined here.

Figure 6 shows the evolution of temperature at the center of the GST layer of sample 2, and Fig. 7 shows different stages of crystallization of this sample, obtained by computer simulations. The laser power for this simulation is assumed to be 8.76 mW in both cases. When the assumed laser pulse has been turned on, the temperature first increases rapidly; it then becomes rather flat; and finally it increases again but slowly. The flat temperature region in Fig. 6 was found to correspond to amorphous-to-crystalline phase transformation. At $t=200$ ns, small crystallites in the central region of the hot spot grow [see Fig. 7 and curve (a) of Fig. 6]. After about 100 ns, the crystallized region expands to about 600 nm in diameter [see Fig. 7 and curve (b) of Fig. 6]. The amorphous regions may transform to crystalline phase either by nucleation of small crystallites and subsequent growth of these crystallites or by the growth at the edge of the crystallized central region. At $t=500$ ns, the size of the crystallized region has grown to about 1 μm in diameter. Interestingly, as

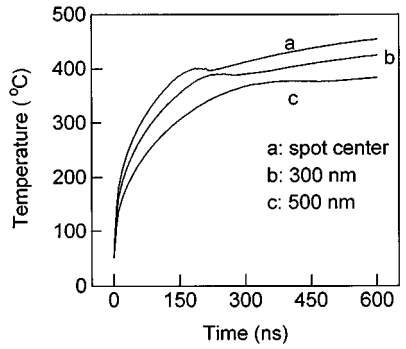

FIG. 6. Calculated temperature vs time at three different locations in the center of the GST layer for the sample 2. The curves labeled (a), (b), and (c) correspond to points at the center of the focused spot, 300 nm away from the center, and 500 nm away from the center, respectively. The assumed laser power is 8.76 mW.

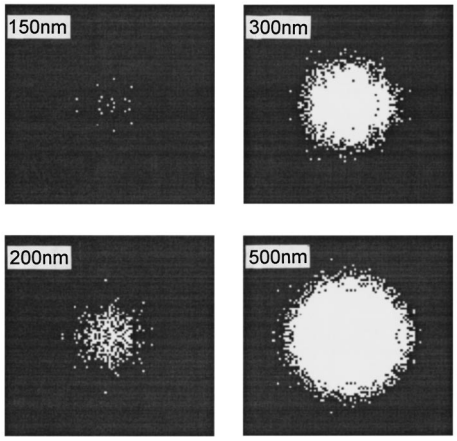

FIG. 7. Crystallization of amorphous phase caused by the irradiation of a focused, 8.76 mW laser beam for sample 2. The dark region represents the amorphous phase, while the bright regions are crystalline phase. The real nuclei size (in area) are only about 1/25 of those displayed. Each frame is 2 μm×2 μm.

seen from Fig. 6, amorphous-to-crystalline phase transition occurs at lower and lower temperatures as time elapses.

D. Amorphization of supercooled liquid

Let us now describe the formation of amorphous marks. We assume that amorphization occurs from melt as it cools down below a certain temperature, T_s, provided that crystallization of the supercooled liquid can be avoided. The choice of T_s, is not an important issue in our simulations, since nucleation and growth of crystals may still proceed in the amorphous region as it does in the supercooled liquid. Here we select $T_s = 250\,^{\circ}\mathrm{C}$ ($T_s = 2T_m/3$ may be more appropriate[2]). Figure 8 shows the variation of temperature with time at three locations in the center of the GST layer of the phase-change disk. From Fig. 8, one can see that the spot center is melted at about 35 ns after the writing pulse has been turned on [see curve (a) of Fig. 9]; the 200 nm off-track location is also melted but at about 15 ns later than the center

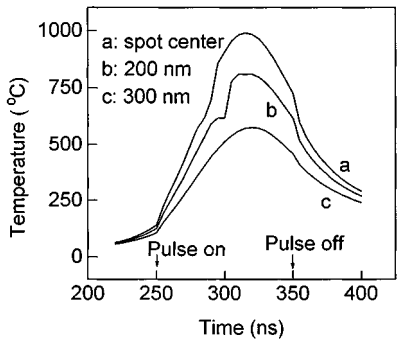

FIG. 8. Calculated temperature vs time at three different locations in the center of the GST layer for the disk: (a) laser spot center location at $t = 300$ ns; (b) 200 nm off-track from the spot center; (c) 300 nm off-track from the spot center. The laser spot was moving at 8.8 m/s along positive x direction. Starting at $t = 0$, the disk was assumed to be illuminated by a focused light of 4.37 mW. At $t = 250$ ns, the laser power was increased to 9.27 mW. After 100 ns, the laser power drops back to 4.37 mW. In the simulations, $r_0 = 410$ nm, $p = 3.69$, $\Delta = 4$ nm, and $\Delta t = 2.5$ ns.

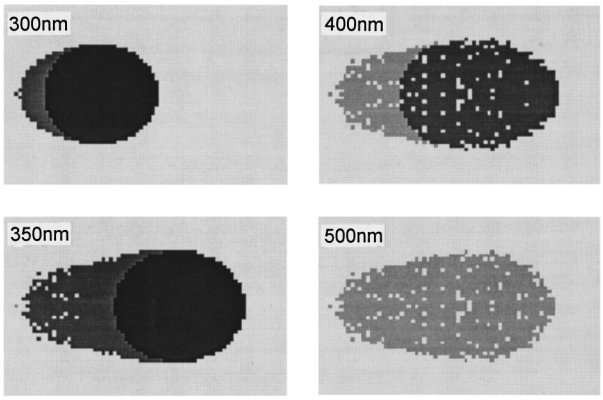

FIG. 9. Formation of an amorphous mark by a 100 ns laser pulse of 9.27 mW starting at $t = 250$ ns. The laser spot moved from left to right at 8.8 m/s. Four different gray regions, from black to bright, represent four different phases: molten pool, supercooled liquid, amorphous region, and crystalline region, respectively. The real nucleus size (in area) is only about 1/25 of those displayed. Each frame is 1.5 μm×1 μm.

[see curve (b) of Fig. 9]. After the 100 ns writing pulse ends, the film cools down. The average cooling rate from melting temperature to 400 °C is around 10^{10} K/s, being fast enough to avoid the crystallization of supercooled liquid. In addition, it is also evident from Fig. 8 that the central site ($y = 0$) has the fastest cooling rate.

Figure 9 shows different stages in the formation of an amorphous mark by a 100 ns laser pulse of 9.27 mW starting at $t = 250$ ns. At $t = 300$ ns, a fairly large region is melted, and the trailing edge of the melted pool has cooled down below the melting point. At $t = 350$ ns, the 100 ns writing pulse ends. The molten pool expands and the supercooled portion also increases. A few nuclei appear in the trailing region. At $t = 400$ ns, the entire molten pool has cooled down to below the melting point; the trailing edge of the molten pool has been transformed to amorphous phase. At $t = 500$ ns, except for dozens of quenched-in nuclei, the molten region has been transformed into an amorphous phase. Moreover, due to the growth from the unmelted edge of the pool, the quenched amorphous mark is slightly smaller than the molten pool. At $t > 500$ ns, the amorphous mark thus formed is stabilized and neither nucleation nor growth occurs inside the mark.

E. Recrystallization of quenched amorphous mark

Figure 10 shows different stages during erasure of an amorphous mark by a 4 mW focused laser beam, obtained by computer simulations. At $t = 250$ ns, the left edge of the mark is under laser exposure, and some of the amorphous regions are recrystallized. As the laser spot moves from left to right, the central regions of the amorphous mark are erased. It is seen that recrystallization is primarily achieved through nucleation and growth within the mark. At $t = 400$ ns, the previously amorphous mark is out of the illuminated region, ending the erasure cycle. The final mark is only partially erased.

Figure 11 shows the relative signal, S_1/S_0, versus erasing power (P_e) for the disk. In the figure, the solid circle represents experimental results, and the open circle stands

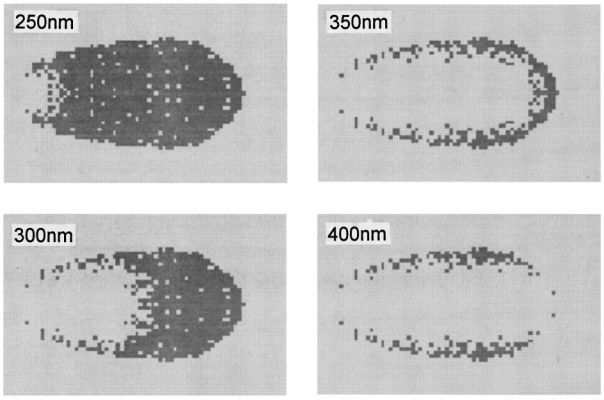

FIG. 10. Recrystallization of an amorphous mark, produced by the irradiation of a 100 ns writing laser pulse of 9.27 mW starting at $t=250$ ns. In the simulations, the laser spot was assumed to move from left to right at a velocity of 8.8 m/s. The optical power for erasure was 4 mW. In the pattern, the dark region represents the amorphous regions, while the bright dotted regions are crystalline phase. Each frame is 1.5 μm$\times$1 μm. The real nuclei size (in area) are only about 1/25 of those displayed.

for simulation results. It is seen that, at $P_e \geqslant 3$ mW, S_1/S_0 begins to drop and amorphous marks are being partially recrystallized (see Fig. 10). At $P_e \geqslant 5$ mW, the amorphous marks are completely erased. But at $P_e > 5.9$ mW, the relative signal increases abruptly. The computer simulations reproduce this behavior quite accurately. Temperature calculation shows that, due to high absorption and low thermal conductivity of the amorphous phase, the local temperature in the amorphous region is higher than that in the crystallized region. At $P_e > 5.9$ mW, the temperature in the amorphous region is so high that the growth probability is low (see Fig. 1). This means that the amorphous region requires a long dwelling time before it may be recrystallized; certain parts of the previously amorphous region are then melted. When the laser spot moves out of the molten regions, the molten pool is again quenched to amorphous phase, resulting in the rise of S_1/S_0. Simulations have also shown that the peak temperature of growth probability determines the critical power for the abrupt increase of S_1/S_0. If the peak temperature of the growth probability curve in Fig. 1 is shifted deliberately to lower temperatures, the laser power for the abrupt rise of S_1/S_0 will be lower. The power margin of erasability depends not only on the multilayer stack, but also on the kinetics of the storage layer.

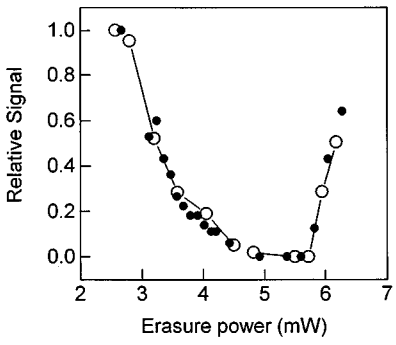

FIG. 11. Variation of relative signal vs erasing power. The experimental results, represented by solid circles, are obtained by erasing the written marks with various erasure power. The simulation results, represented by open circles, are obtained by erasing a computer-produced mark using various erasure power. The solid line, which connects the open circles, is a guide to the eye.

V. CONCLUSIONS

We have described the numerical procedures for temperature calculation of laser-induced local heating of multilayers in three-dimensional space and modeled the crystallization kinetics for phase-change rewritable media. Experiments have been used to indirectly determine the probabilities of nucleation and growth for $Ge_2Sb_2Te_5$ alloy. Some fundamental aspects in phase-change erasable storage, such as the crystallization of the as-deposited amorphous phase, amorphization of supercooled liquid, and recrystallization of quenched amorphous phase have been addressed based on the three-dimensional temperature calculations and our kinetics model. The calculated transient reflectance of the as-deposited amorphous phase for a single GST layer and for a quadrilayer stack, as well as erasability for a GST quadrilayer disk are in good agreement with experimental results within the laser power range studied.

ACKNOWLEDGMENT

We would like to thank Dr. Takeo Ohta of the Matsushita Electric Company of Japan for providing the phase-change samples and the disk for our experiments.

[1] J. Feinleib, J. de Nuerville, S. C. Moss, and S. R. Ovshinsky, Appl. Phys. Lett. **18**, 254 (1971).
[2] M. Libera and M. Chen, MRS Bull., April, 40–45 (1990).
[3] N. Yamada, E. Ohno, K. Nishiuchi, and N. Akahira, J. Appl. Phys. **69**, 2849 (1991).
[4] T. Ohta, K. Yoshioka, H. Isomura, and T. Akiyama, Proc. SPIE **2514**, 302 (1995).
[5] H. Iwasaki, M. Abe, B. Jacobs, and A. Dewey, Proc. SPIE **2514**, 200 (1995).
[6] D. J. Gravesteijn, Appl. Opt. **27**, 736 (1988).
[7] Y. Nakayoshi, Y. Kanemitsu, Y. Masumoto, and Y. Maeda, Jpn. J. Appl. Phys., Part 1 **31**, 471 (1992).
[8] Q. M. Lu and M. Libera, J. Appl. Phys. **77**, 517 (1995).
[9] Z. L. Mao, H. Chen, and Ai-Lien Jung, J. Appl. Phys. **78**, 2338 (1995).
[10] J. H. Coombs, A. P. J. M. Jongenelis, W. van Es-Spiekman, and B. A. J. Jacobs, J. Appl. Phys. **78**, 4906 (1995).
[11] T. Ohta, K. Inoue, M. Uchida, K. Yoshioka, T. Akiyama, S. Furukawa, K. Nagata, and S. Nakamura, Jpn. J. Appl. Phys., Part 1 **28**, Suppl. 28, 123 (1989).
[12] H. Yasuoka, M. Ojima, M. Terao, and T. Nishida, J. Appl. Phys. **26**, Suppl. 26–4 (171,1987).
[13] H. Minemura, H. Andoh, N. Tsuboi, Y. Maeda, and Y. Sato, J. Appl. Phys. **67**, 2731 (1990).
[14] Y. Maeda, I. Ikuta, H. Andoh, and Y. Sato, Jpn. J. Appl. Phys. Ser. 6, 58 (1991).
[15] H. S. Carslaw and J. C. Jaeger, *Conduction of Heat in Solids* (Oxford University Press, London, 1954).
[16] M. Mansuripur, G. A. N. Connell, and J. W. Goodman, Appl. Opt. **21**, 1106 (1982).
[17] M. Mansuripur and G. A. N. Connell, Appl. Opt. **22**, 666 (1983).
[18] R. J. Anderson, J. Appl. Phys. **64**, 6639 (1988).
[19] A. H. M. Holtslag, J. Appl. Phys. **66**, 1530 (1989).
[20] W. A. McGahan and K. D. Cole, J. Appl. Phys. **72**, 1362 (1992).
[21] O. W. Shih, J. Appl. Phys. **75**, 4382 (1994).

[22] W. H. Press, B. P. Flannery, S. A. Teukolsky, and W. T. Vetterling, *Numerical Recipes in C* (Cambridge University Press, London, 1989).
[23] C. A. Paddock and G. L. Eesley, J. Appl. Phys. **60**, 285 (1986).
[24] J. Burke, *The Kinetics of Phase Transformations in Metals* (Pergamon, New York, 1965).
[25] K. F. Kelton, J. Non-Cryst. Solids **163**, 283 (1993).
[26] D. R. Uhlmann, *Advances in Nucleation and Crystallization in Glasses*, edited by L. L. Hench and S. W. Freiman (American Ceramic Society, Columbus, Ohio, 1971).
[27] A. E. Owen, in *Amorphous Solid and the Liquid State*, edited by N. H. March, R. A. Street, and M. Tosi (Plenum, New York, 1985).
[28] J. W. Cahn, Acta Metall. **8**, 554 (1960).
[29] L. Cheng and M. Mansuripur, Optical Data Storage Topical Meeting '97, paper No. WB4.
[30] M. Mansuripur, C. Peng, J. K. Erwin, W. B. Bletscher, S. G. Kim, S. K. Lee, R. E. Gerber, C. Bartlett, T. D. Goodman, Lu Cheng, C. S. Chung, T. K. Kim, and K. Bates, Appl. Opt. (to be published).